# STELLAR OCCULTATIONS BY SMALL BODIES: DIFFRACTION EFFECTS

F. ROQUES
Observatoire de Paris, 92190 Meudon, France

M. MONCUQUET
Université Paris VI, 9 Quai Saint-Bernard, 75005 Paris, France

B. SICARDY
Observatoire de Paris, 92190 Meudon, France
and
Université Paris VII, 2 Place Jussieu, 75005 Paris, France

*Received 28 October 1986; revised 7 January 1987*

## ABSTRACT

In recent years, stellar occultations have been a powerful tool in the study of small bodies of the solar system (e.g., rings, satellites, asteroids). Diffraction effects have to be taken into account in order to interpret light curves. We develop here theoretical models, from the Fresnel-Kirchhoff diffraction theory, of occultations by semitransparent strips and opaque elliptical disks, and we give explicit methods for computing them. We discuss the theoretical implications of diffraction during stellar occultations and use our own models to distinguish the dips that are artifacts from those that can correspond to real planetary objects. We apply these considerations to some observations of Uranus' rings and Neptune's arcs.

## I. INTRODUCTION

Observation of stellar occultations by solar system objects has proved to be an efficient method of studying both the occulting objects and the occulted stars. This technique consists in recording, with high-speed photometry (typically 10 ms), the stellar flux when an object approaches the star and then occults it on the celestial sphere. A general advantage of these observations is the high spatial resolution they achieve, in addition to the possible discovery of material otherwise seen only with difficulty from the ground. Let us briefly recall two important applications of such a method (see Sec. V for more details):

(1) Occultations by the Moon, which allow estimates of the sizes of the stars as well as the detection of double stars (Nather and Evans 1970). Regular observations have led to the discovery of double stars, even down to vector separations of a few thousandths of an arcsecond, and have yielded data on magnitude differences between the companions (Evans 1984).

(2) Occultations by the planets, which yield important results about planetary stratospheres and environments (Elliot 1979). The arcs of Neptune were discovered in this way (Hubbard *et al.* 1986), as well as the rings of Uranus (Elliot *et al.* 1977), the positions of which are now known with an accuracy of a few hundred meters (French *et al.* 1986).

Theoretical models taking light diffraction into account have been successfully used for analyzing occultation data. In particular, models of occultation by semitransparent rings have been already used to study the Uranus system and have given very precise values of widths and optical depths (Hubbard and Zellner 1980; Elliot *et al.* 1984). On the other hand, during occultations by the remote planets, the recorded light curves often exhibit dips, and there has been a great deal of interest recently in their interpretation.: Are they real planetary objects (i.e., ring structures or satellites), or artifacts (e.g., electrostatic or guiding problems, seeing fluctuations)? Because of their characteristic shape, many artifacts can be eliminated. The apparent size of the occulted star provides a minimal width to an occultation profile. Diffraction effects, which give a minimal width for a "real" event (the Fresnel scale, defined in Sec. II), provide another important test. Nevertheless, some dips "resist" these kinds of analysis; thus, in order to test these isolated events and also to discuss theoretical bases of previous diffracting models, we have been induced to study, in a general way, the diffraction pattern produced by small occulting objects, rings, or solid bodies.

The aim of this paper is (i) to present and justify numerical algorithms necessary for generating diffraction patterns (such algorithms can be implemented on mini- or microcomputers) and (ii) to discuss the theoretical implications of diffraction during observations of stellar occultations. The diffraction theory is presented in Sec. II. The diffraction pattern of rectangular objects is easily obtained in terms of the "Fresnel" functions. An algorithm for the calculation of these functions with arbitrary precision is presented in Appendix A. Generalizing the rectangle formula when one or several edges are infinite, diffraction patterns of a strip and a "grey" strip (the square-well ring model, cf. Elliot *et al.* 1984) are derived in Sec. III. The diffraction pattern of a complex body can be constructed from an addition of simple rectangles, and, using this method, the diffraction patterns of circular or elliptical objects (moonlet model) are presented in Sec. IV. The circular case can be treated directly with the "Lommel" functions (Appendix B). In the last section (V), we review how diffraction is taken into account in the analysis of stellar occultation data, namely for occultations by the Moon, asteroids, and semitransparent rings (in the last case, we discuss optical-depth interpretation when measured from the Earth or from a spacecraft). Finally, we present some examples of applications of our models to the analysis of occultations by Uranus' rings and Neptune's arcs.

## II. DIFFRACTION THEORY

The diffraction pattern of a planar wave produced by an object with abrupt edges will be calculated as a proper case of Fresnel diffraction, expressed from Kirchhoff's diffraction theory.

Fresnel diffraction refers to the diffraction phenomena obtained at *finite* distance by application of the Huygens-

 0004-6256/87/061549-10$00.90  

Fresnel principle of wave propagation: each point of a wave front may be considered as the center of a secondary disturbance giving rise to spherical wavelets, which mutually interfere. If part of the original wave front is blocked by an obstacle, the system of secondary waves is incomplete, so that diffraction occurs. From a less intuitive point of view, Kirchhoff has built up a diffraction theory on the basis of the homogeneous scalar-wave equation of Helmholtz, which embodies the Huygens-Fresnel principle and describes explicitly the variation of the amplitudes of secondary waves as a function of the direction. This theory is entirely adequate for problems where the dimensions of diffracting obstacles are large compared to the wavelength and small compared to the distance of observation (cf. Born and Wolf 1980, Chap. VIII).

The occulting object is represented as an opaque flat surface $S$ (i.e., we assume that intercepted light is entirely absorbed and there is no scattering by the edges) located at a large distance $D$ from the observer (but not too large to remain in the frame of Fraunhofer diffraction, see Born and Wolf 1980, p. 382). $S$ lies in a plane $P$ perpendicular to the line of sight (denoted by $0-S$, see Fig. 1). If we choose as origin of $P$ the intersection $M$ with the line of sight $0-S$, then the complex diffracted amplitude $a_S$ of an incident monochromatic plane wave of wavelength $\lambda$ is given, at the observation point 0, by the Fresnel-Kirchhoff diffraction formula

$$a_S(0) = N \int\int_{P-S} \frac{e^{\frac{2i\pi}{\lambda}(\sqrt{X^2+Y^2+D^2}-D)}}{\sqrt{X^2+Y^2+D^2}} \times (1+\cos\theta)\,dX\,dY, \quad (1)$$

where $P-S$ denotes the complement of $S$ in $P$, $\theta$ is the angle of diffraction, and $N$ is a complex normalizing parameter which ensures $a_S(0)=1$ when $S$ vanishes; i.e., when there is no object. We will see in the next section that $N = 1/2\lambda i$.

When both the dimension of $S$ and its distance to $M$ are small compared to $D$ (i.e., $X^2+Y^2 \ll D^2$), the normalized amplitude diffracted by $S$ reads

$$a_S(0) = 1 - \frac{2N}{D}\int\int_S e^{\frac{i\pi}{\lambda D}(X^2+Y^2)}\,dX\,dY. \quad (2)$$

Expression (2) is well adapted to the calculation of the diffraction by a rectangular screen $R$. Consider a Cartesian reference frame with fixed origin $0'$ in $P$ and $0'x$, $0'y$ axes parallel to the sides of rectangle $R$. We denote by $(x_1, y_1)$ and $(x_2, y_2)$ the minimum and maximum coordinates of $R$, respectively, and by $(x,y)$ the coordinates of $M$. The integral (2) now reads

$$a_R(x,y) = 1 - \frac{2N}{D}\int_{x_1-x}^{x_2-x} e^{\frac{i\pi}{\lambda D}X^2}\,dX \int_{y_1-y}^{y_2-y} e^{\frac{i\pi}{\lambda D}Y^2}\,dY, \quad (3)$$

and choosing $\sqrt{\lambda D/2}$ as length unity (Fresnel scale), we obtain

$$a_R(x,y) = 1 - N\lambda\,[F(x_2-x) - F(x_1-x)] \times [F(y_2-y) - F(y_1-y)], \quad (4)$$

where $F(x)$ is the complex Fresnel function defined by

$$F(x) = \int_0^x e^{\frac{i\pi}{2}X^2}\,dX.$$

We have developed an algorithm which allows one to compute $F$ with arbitrary accuracy, and which is easily usable even with a small computer (see Appendix A).

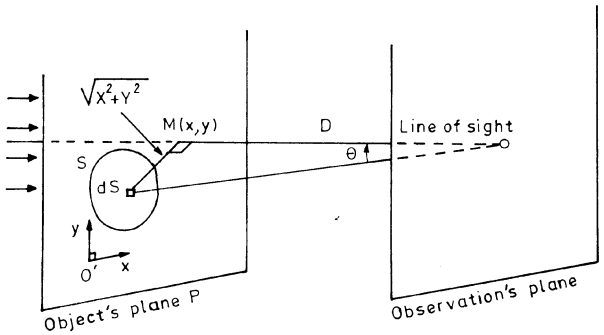


FIG. 1. Geometry of Fresnel diffraction.

## III. DIFFRACTION BY A STRIP: CASE OF THE OCCULTATION BY A RING

Equation (4) enables one to compute the diffracted intensity $I = |a|^2$ not only for rectangular screens of small sizes, but for all limiting cases (half-plane, rectangular wedge, strip, or truncated strip) near the edge, by use of the asymptotic values: $F(+\infty) = -F(-\infty) = \frac{1}{2}(1+i)$. However, this point needs further explanation. Actually, it seems rather contradictory to let a dimension of the rectangle go to infinity and to apply the formulas (2) and (4), where we assumed small surfaces; i.e., $X^2+Y^2 \ll D^2$. It is possible to avoid this problem by using for these infinite screens a rigorous (expressed from Maxwell's equations) diffraction theory introduced by Sommerfeld for the perfectly conducting half-plane. This theory confirms the validity of Fresnel's approximations, particularly for optical wavelengths out of the screen plane and its vicinity (Born and Wolf 1980, Chap. XI). Nevertheless, we will briefly show why we can use Eq. (2) instead of Eq. (1) even for asymptotic cases: the key point is that only a small neighborhood of the origin (where $X^2+Y^2 \ll D^2$) contributes effectively to the result of an integration of Eq. (1) on an *infinite* domain. The asymptotic part cancels out because the phase of the integrand varies very rapidly.

If, for instance, $Y$ goes to infinity in Eq. (1) when $X$ is fixed and negligible compared to $D$, we must then evaluate

$$\int_0^{+\infty} \frac{e^{\frac{2i\pi}{\lambda}(\sqrt{Y^2+D^2}-D)}}{Y^2+D^2}(\sqrt{Y^2+D^2}+D)\,dY. \quad (5)$$

We can avoid the complex exponential by substituting $Y = Du\sqrt{u^2+2}$ and by integrating along the edges of the sector $0 < Arg(z) < \pi/4$ in the complex plane. Then integral (5) is given by

$$2\int_0^{+\infty} e^{\frac{-2\pi D}{\lambda}t^2} \frac{\sqrt{t^2-2i}}{t^2-i}\,dt,$$

where $\sqrt{t^2-2i}$ is the principal determination of the square root. So, owing to the very large size of the factor $\sqrt{2D/\lambda}$, this integral is virtually equal to $\sqrt{\lambda/D}\,e^{i\pi/4}$, which is the result we obtain if we consider $Y$ negligible compared to $D$, as in Eq. (2). Thus, Eq. (4) gives the diffracted amplitude produced by rectangular screens of small and/or infinite dimensions. In particular, this equation is valid when the screen is the whole plane, and we obtain in this case

$N\lambda\,[2F(\infty)]^2 = 1$, i.e., $N = 1/2\lambda i$.

Now, for an opaque strip of halfwidth $w$, we have

$$a_w(x) = 1 + \tfrac{1}{2}(i-1)[F(w-x) + F(w+x)], \quad (6)$$

and writing $F(x) = C(x) + iS(x)$,

$$I_w(x) = \tfrac{1}{2}\{[C(w-x) + C(w+x) - 1]^2 + [S(w-x) + S(w+x) - 1]^2\}. \quad (7)$$

It is straightforward to compute the intensity of light when the occulting body is *homogeneously* semitransparent; that is, it removes a fraction $p$ ($0 < p \leqslant 1$) of the amplitude of the wave at any point of its surface. Then the intensity transmitted by such a "grey strip" is

$$I_{w,p}(x) = \tfrac{1}{2}\{[p\,C(w-x) + p\,C(w+x) - 1]^2 + [p\,S(w-x) + p\,S(w+x) - 1]^2\}. \quad (8)$$

In fact, a planetary ring is not a homogeneous grey strip but is composed of a large number of small diffracting opaque particles. In this case the value of the formal opacity parameter $p$ is discussed by Cuzzi (1985) and reanalyzed in Sec. V.

Examples of theoretical light curves calculated with Eqs. (7) or (8) are in Elliot *et al.* 1984 (in the Appendix) and in this paper Fig. 4 (profile (c)).

## IV. DIFFRACTION BY ELLIPTIC SCREENS: CASE OF THE OCCULTATION BY A LITTLE SATELLITE OR AN ASTEROID

It is of interest to construct diffraction patterns caused by more realistic objects than "parallelepipeds" of the previous section, such as moonlets or asteroids. We can think of spherical bodies, but also of ellipsoids or merely irregular bodies.

We first consider an opaque disk of radius $\rho$. In the plane of the object, we use polar coordinates, denoted by $(R,\varphi)$, with fixed origin 0′ at the center of the disk, and argument origin 0′$M$ (Fig. 1). We denote $\|\mathbf{0'M}\|$ by $r$; thus the optical path difference becomes $X^2 + Y^2 = R^2 + r^2 - 2Rr\cos\varphi$, and carrying in Eq. (2), we obtain

$$a_\rho(r) = 1 - \frac{2\pi e^{\frac{i\pi}{\lambda D}r^2}}{\lambda D i}\int_0^\rho e^{\frac{i\pi}{\lambda D}R^2} J_0\left(\frac{2\pi}{\lambda D}rR\right) R\,dR, \quad (9)$$

where

$$J_0(x) = \frac{1}{\pi}\int_0^\pi \cos(x\sin t)\,dt$$

is the Bessel function of zero order.

The function to be integrated oscillates more and more rapidly as $R$ increases, invalidating usual integration algorithms for practical calculations. Lommel (1884) gave a complete analytical solution of such a problem using the so-called Lommel's functions: we outline in Appendix B the principle of his method and give the solutions expressed with our notations. We have implemented this method on computers: it yields good results but rather slowly near the edge of the geometric shadow, where the alternate series of Bessel functions, which defines the Lommel functions, have many significant terms (see Eq. (B3) in Appendix B). On the other hand, our specific problem of occultation by a moonlet or an asteroid does not need a perfect circular model but rather a sufficiently isotropic diffraction pattern, in which the light intensity mainly depends on $r$. Furthermore, it is actually interesting to extend the calculation to elliptical bodies, which is not possible from Eq. (9).

For these reasons, we have developed a numerical integration of Eq. (2) on a circular or elliptical screen, directly inferred from the rectangular case, for which a fast algorithm is available. We consider a circle or an ellipse, which will be the model's envelope, and a Cartesian reference system with fixed origin at its center. The model is composed of joined rectangles whose edges are parallel to the reference axes and constructed as follows (see Fig. 2).

We divide the arc $(0,\pi/2)$ in successive powers of 2, so that, at step $n$, we have determined $2^n - 1$ points on this arc. Each of these points defines the maximum coordinates of a rectangle. To obtain the complete model, we finally make two symmetries with respect to the reference axes (note that we omit some rectangles which have negligible contributions: their exact number is indicated in the caption to Fig. 2).

The calculation of Eq. (2) for four rectangular screens symmetric with respect to the reference axes, from a positive coordinates rectangle $(x_1, y_1)$ and $(x_2, y_2)$ (see the hatchings in Fig. 2), can be simplified using a complex function $f$ defined, in units of Fresnel scale, by

$$f(x,x_j) = \int_{x-x_j}^{x+x_j} e^{\frac{i\pi}{2}X^2}\,dX = F(x+x_j) - F(x-x_j),$$

and we obtain the contribution to the amplitude from these four symmetric rectangles (denoted $\hat{a}$) by

$$\hat{a}(x,y) = \tfrac{i}{2}[f(x,x_2) - f(x,x_1)][f(y,y_2) - f(y,y_1)]. \quad (10)$$

At a given step $n$, the $f(x,x_1)$ and $f(y,y_1)$ terms have been already calculated, so that calculation of $\hat{a}(x,y)$ needs only four further Fresnel integral values. Consequently, the complete model needs a number of Fresnel integral calculations that is equal to the number of considered rectangles (twice less if the envelope is a circle, because of symmetry with respect to the frame's diagonals).

The choice of $n$, which can be regarded as an irregularity factor, mainly depends on the obstacle size. To control how the method converges, we first computed the diffraction pattern of a circular screen; we consider the multirectangle model suitable when the diffracted-light intensities computed along two radial axes of argument 0 and $\pi/4$ do not differ more than a given tolerance (the most different profiles of intensity are obtained along these axes). It appears that the parameter $n$ must be increased to ensure a given tolerance when the object's radius increases. We have indicated in Fig. 3 the maximum allowable radii (in Fresnel scale units) in order not to exceed 5% or 1% of error of the model "isotropy." Otherwise stated, small *irregular* objects (i.e., with small $n$) can reproduce the diffraction pattern of disks, including the presence of a central spot (see below and Fig. 4).

Furthermore, we have checked that, for adequate $n$, the direct integration of Eq. (9) with Lommel's method (Appendix B) and the multirectangle models for circular disks are in excellent agreement. We noted that the multirectangle calculation requires less computer time than Lommel's method for small disks—i.e., radius less than 1.5 times the Fresnel scale—and also for larger disks near the edge of the geometric shadow.

Finally, when $n$ is adequate for a disk, we assume that its value is also adequate for elliptical screens of comparable size.

Some occultation profiles produced by squares, strips, disks, and ellipses are presented in Figs. 4 and 5 and dis-

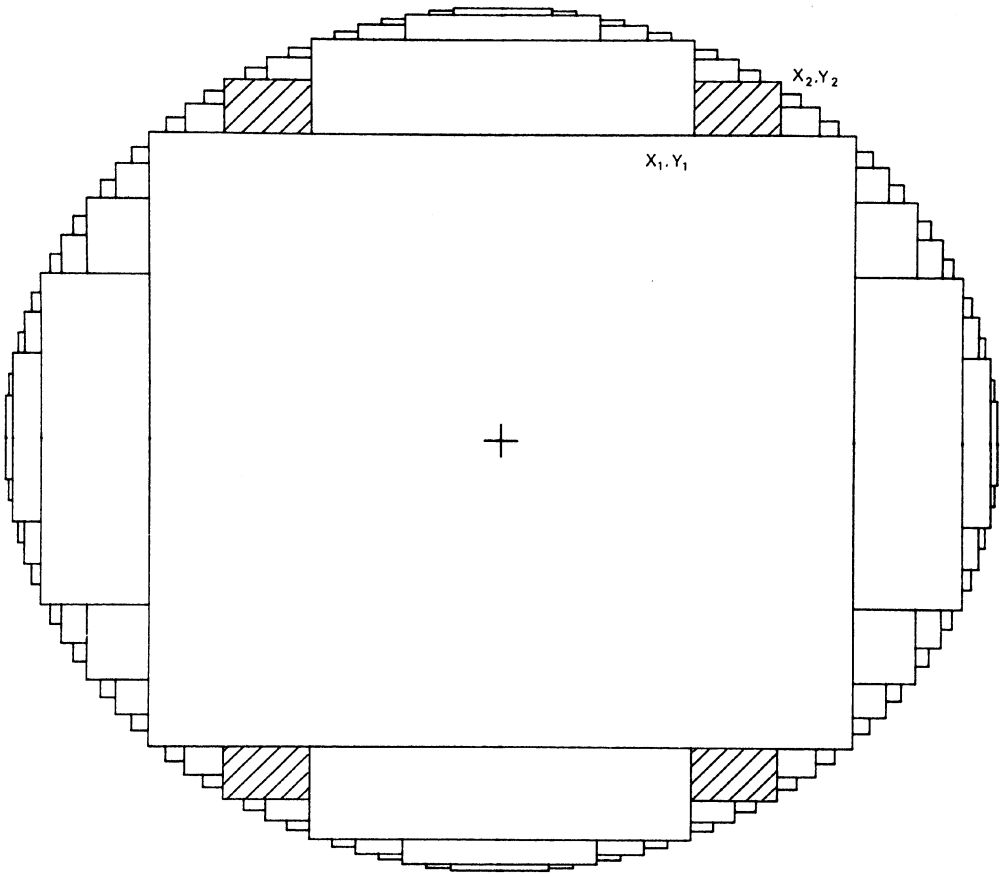


FIG. 2. Elliptical object model ($n = 5$). We do not take into account, to obtain the model "$n$," the rectangles whose areas are less than the greatest rectangle area of step $n + 1$. The following table gives the exact number of rectangles considered for each step $n$; that is, the number of Fresnel functions calculated to obtain a point of the profile (rectangles over frame axes are counted for two):

| $n =$ | 2 | 3 | 4 | 5 | 6 | 7 | 8 | 9 | 10 |
|---|---|---|---|---|---|---|---|---|---|
| | 12 | 28 | 60 | 116 | 236 | 468 | 932 | 1868 | 3724 |

cussed in their captions. The most obvious property of circular disk profiles is the presence of a central flash (the so-called Poisson spot) whose intensity is equal to 1, as if no screen were present. This result is easy to predict using Eq. (9) with $r = 0$. The area of this central flash decreases when the size of the object is increased. From the Lommel formula (see Appendix B), we see that the first zero of the Poisson spot is given by $J_0(\pi\rho r) = 0$, and so the radius of the spot is given by $0.76/\rho$ Fresnel scale, if $\rho$ is the radius of the object, also in Fresnel scale. In the case of an elliptical obstacle, the Poisson spot decreases when the eccentricity increases, but it depends, too, on the object size: A numerical study shows that its maximum intensity is higher than 0.5 if the product of the object semimajor axis (in Fresnel scale units) by the eccentricity is less than $\sim 1.2$.

## V. PHYSICAL APPLICATIONS TO STELLAR OCCULTATIONS

### *a) Occultations by the Moon*

Stellar occultations by the Moon are widely used to detect double stars, to measure the limb-darkened angular diameter of the occulted stars (see, for example, Ridgway *et al.* 1979), and, more recently, to study stars with emission shells (White and Slettebak 1980). Diffraction effects are necessarily taken into account in these observations, for which the Fresnel scale in visible wavelengths is about 10 m, and a deep study of the lunar limb effect has been made by Evans (1970). Nevertheless, the lunar limb is merely modeled by a half-plane single edge, because, as Evans points out, it is difficult to refine this model and to separate the effects of the irregular lunar surface and of the stellar properties. On the basis of diffraction by a half-plane single edge, Nather and McCants (1970) give appropriate models for the analysis of lunar occultation data and the procedure for model fitting, using nonlinear least-squares techniques.

### *b) Occultations by Asteroids*

Observations of stellar occultations by asteroids provide accurate sizes and shapes of the objects, via comparison of the different emersion and immersion timings from different sites (for instance, this method gives Ursula's diameter as $216 \pm 10$ km, Millis *et al.* 1984). Secondary events observed during occultations can be interpreted as satellites (Arlot *et*

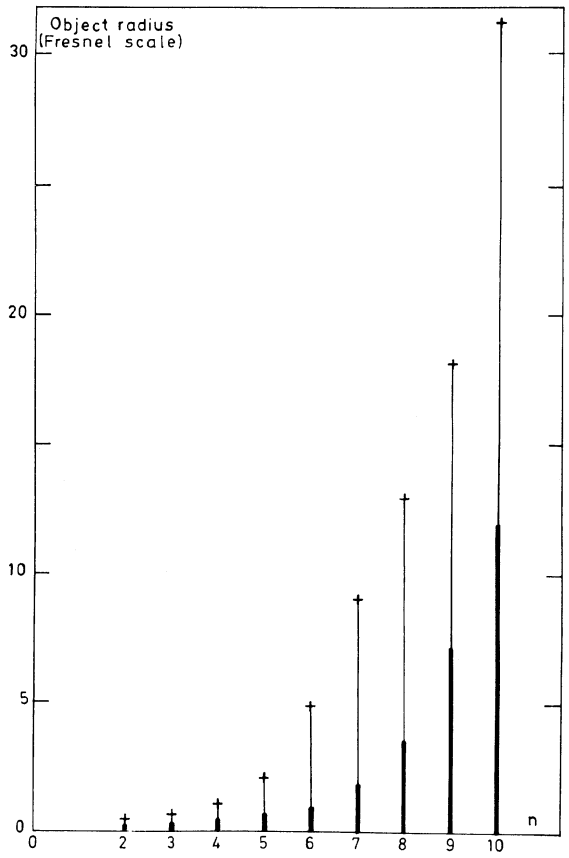


FIG. 3. Radii of circular objects allowable for each step $n$ and for isotropy tolerances of 1% (heavy lines) and 5%.

*al.* 1985). Diffraction is very important during asteroid occultations (the Fresnel scale in visible wavelengths is about 300 m) and the fringes have already been observed (Lecacheux 1986) but have never been used to study asteroids. Indeed, such a study should require high-quality occultation recordings, quite rare because the objects are small, so that catching the event from a large telescope is difficult. We note that, even if the asteroid is sufficiently smooth and circular, the chance to observe the Poisson spot during such an observation is vanishingly small, because the size of the spot does not exceed a few meters for typical asteroids.

### *c) Occultations by the Planets*

Stellar occultations by remote planets like Uranus and Neptune are a very efficient method for studying the surroundings of these planets, including rings, isolated objects, and diffuse matter. A very good knowledge of the position and the width of the Uranian rings has now been achieved (Nicholson *et al.* 1982; Elliot *et al.* 1984; French *et al.* 1986): the error in position is less than one kilometer for objects virtually invisible from the Earth.

Our group has observed a certain number of occultations by Uranus and Neptune which exhibit several dips, sometimes corresponding to known rings and sometimes not (isolated events) (Roques 1986). In order to test these dips and to study the characteristics of the small occulting objects, we have developed a diffraction model of occultation profiles by semitransparent rings and by isolated opaque and spherical objects. The synthetic profiles are computed, for a point light source at a given wavelength, with methods given in Secs. III and IV. The profile is then convolved with the filter bandwidth and the stellar disk (which can have an adjustable size, see below). The limb-darkening parameter is *not* used. These synthetic profiles are used to fit by least squares the recorded occultation profiles. This correlation gives the midtime of the occultation and the best values of the two free parameters of the synthetic profile, which are, for a ring, its width and its opacity (projected in the sky plane), and for a circular object its radius and the impact parameter of the encounter.

In the special case of a ring profile, width and opacity must be corrected for physical interpretation. For the width it is enough to take into account the angle between the star path and the ring perpendicular, but the interpretation of ring opacity needs further explanation.

The opacity parameter $p$ is simply related to the optical depth of the ring $\tau$ by $(1-p)^2 = f = e^{-\tau}$, where $f$ denotes the fractional transmitted energy. These parameters must then be corrected to take into account the elevation angle $B$ of the line of sight with the plane of the studied ring. We finally obtain the normal fractional transmission $f_n$ and the normal optical depth $\tau_n$ by the relation (see Elliot *et al.* 1984) $\tau_n = \tau \sin B$ if we assume the ring is many particles thick (polylayer), and $(1-f_n) = (1-f)\sin B$ if we assume the ring forms a monolayer without significant shadowing, i.e., with $B$ close to 90°. Now, the key point to physical interpretation of these formal parameters is that the transmitted energy measured from the Earth depends not only on the fractional area covered by the particles but also on a diffraction effect induced by each ring particle. The importance of diffraction by the ring particles has been pointed out by Cuzzi (1985). He underlines that the optical depths derived for the Uranian rings during stellar occultations (observed from the Earth) are twice the actual optical depths, which was confirmed during the *Voyager* PPS occultation experiment (Lane *et al.* 1986). This can be shown by using a slightly different approach than Cuzzi.

Let us consider a ring of area $S$, composed of particles which cover a total area $s$, so that the fractional covered area is $s/S$, corresponding to an optical depth $e^{-\tau_0} = 1 - s/S$. Clearly, such a ring removes a fraction $s/S$ of the total incident energy. Consequently, the integral in Eq. (2) is the sum of many integrals, each of them corresponding to one particle. Assuming that the radius $r$ of the particles is small compared to the Fresnel scale, $\sqrt{\lambda D/2}$, $a_S(0)$ may be rewritten

$$a_S(0) = 1 - \frac{2N}{D}\sum_{k=1}^{\mathcal{N}} e^{\frac{i\pi}{\lambda D}(X_k^2 + Y_k^2)} \times \iint_{S_k} e^{\frac{2i\pi}{\lambda D}(uX_k + vY_k)}\, du\, dv\,, \qquad (11)$$

where $u,v$ are the coordinates measured from the center $X_k$, $Y_k$ of the $k$ th particle and $\mathcal{N}$ is the number of particles.

So it appears that the observed profile is the interference figure of many elementary diffraction patterns represented by the integrals in Eq. (11). The width of these diffraction patterns is $\sim\lambda D/r$, typically several thousand kilometers at the Earth, with $r \sim 1$ m. If the width of the rings is small compared to $\lambda D/r$, and if we remain close to the geometric

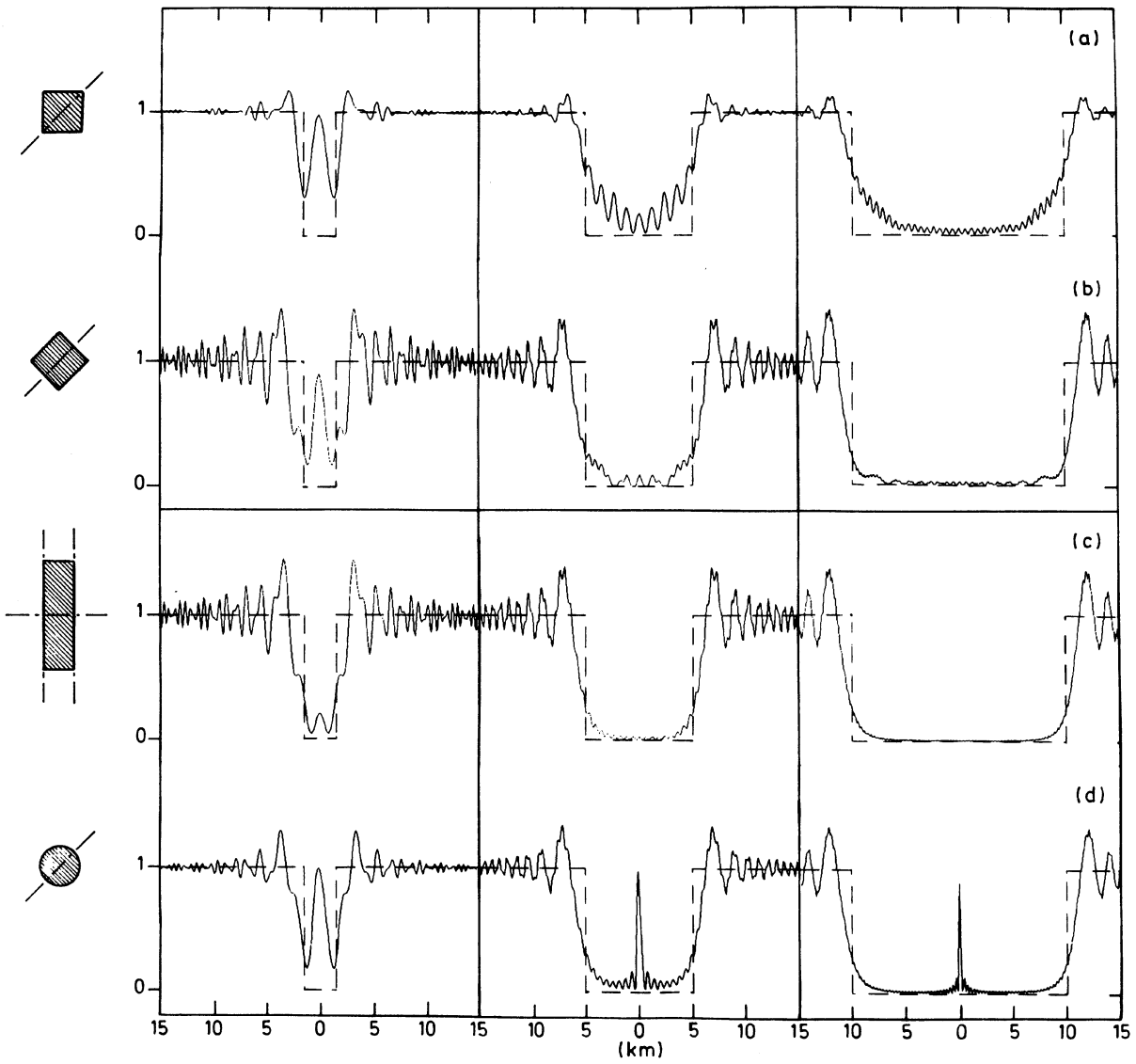


FIG. 4. Occultation profiles with diffraction for a point source, produced by squares, strips, and circular disks. Upper panels show profiles produced by square screens when the source is kept along a diagonal (profile (a)) and along a median line (profile (b)). Lower panels show profiles produced by opaque strips when the source is kept along a perpendicular line to the edge (profile (c)), and by quasicircular objects (profile (d)) along a radial axis, with $n$ such that we ensure an isotropy better than 1%. In each of these cases, we show three object sizes: 1.5, 5, and 10 km halfwidth of geometrical shadow (indicated by dotted lines), with 1.7 km Fresnel scale corresponding to Uranus distance at $\lambda = 2.2$ $\mu$m. We see that the amplitude of the fringes is very attenuated when the source immerses behind a rectangular wedge (profile (a)) compared to the fringes produced when the source immerses behind a straight edge (profiles (b) and (c)). For small squares (1.5 km), we note a central flash of almost 1 intensity which is much greater than in the strip case (c). For broader cases, (b) and (c) profiles are quite similar (and so not very different from profiles produced by a half-plane single edge). In circular cases (profile (d)), the Poisson spot, of exactly unit intensity, is produced by any object size, but its width decreases when the object size increases. For 1.5 km radius, the profile (d) is a middle term between the profiles (a) and (b). For greater radii, the fringes are not very different from ones produced by strips, or squares (or half-planes) along a line perpendicular to the edge, except for the Poisson spot.

shadow of the ring, then each integral in Eq. (11) is equal to unity, so that

$$a_S(0) = 1 - \frac{2N}{D}\frac{s}{S}\iint_S e^{\frac{i\pi}{\lambda D}(X^2+Y^2)}\,dX\,dY. \qquad (12)$$

Otherwise stated, the ring which initially removes a fraction $s/S$ of the *energy* is now equivalent to a uniform grey strip which removes a fraction $s/S$ of the *amplitude*. Consequently, the energy transmitted by the ring, $f_0 = 1 - s/S$, is the square root of the energy transmitted by the profile $f = (1 - s/S)^2$, and the derived optical depth $\tau = -\ln(1 - s/S)^2$ is twice the actual optical depth $\tau_0 = -\ln(1 - s/S)$. The energy difference $(1 - s/S)s/S$ is lost over a much larger scale than the ring width, and is thus indistinguishable from the noise of the signal.

### *d) Some Examples*

We have analyzed two occultations by Uranus, on 15 August 1980 and 22 April 1982. The 1982 occultation has been

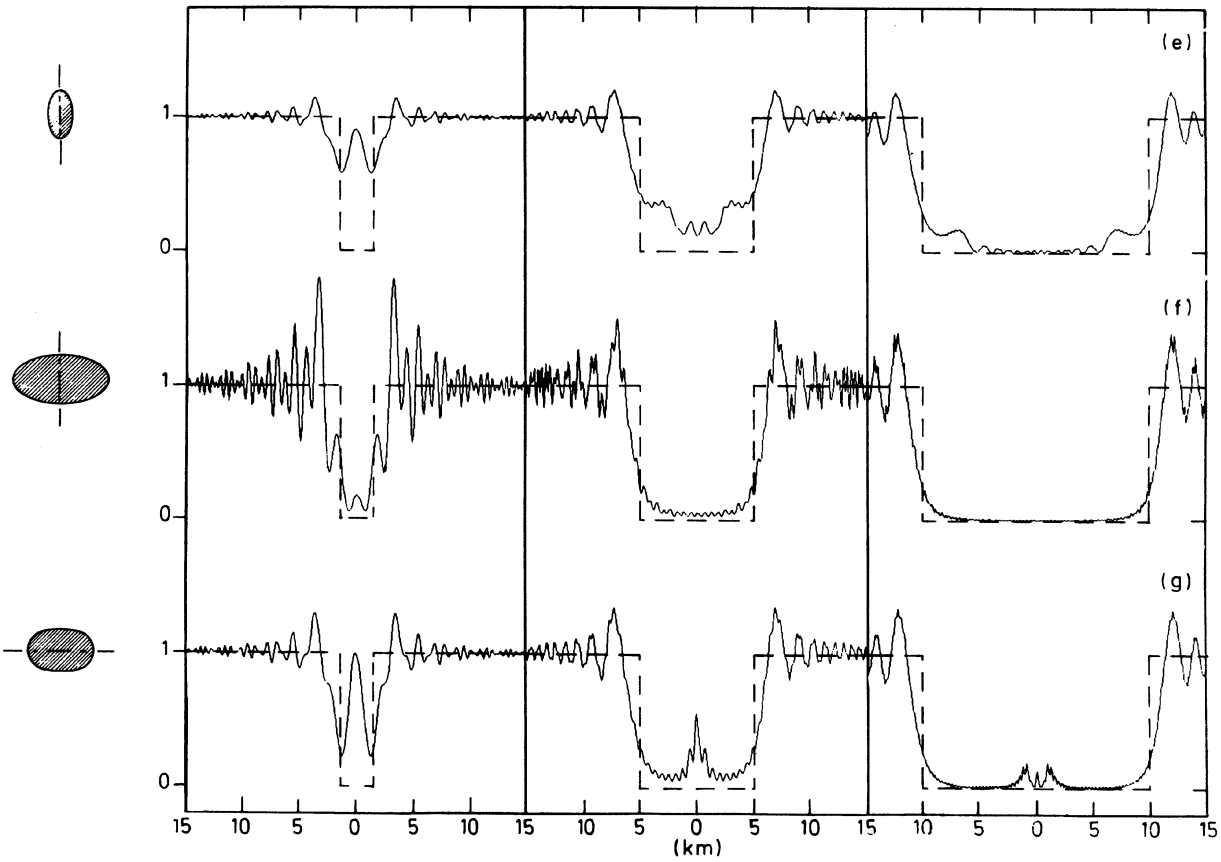


FIG. 5. Occultation profiles with diffraction for a point source, produced by elliptical disks. This figure shows profiles produced by opaque elliptic screens when the source is kept along the major axis (profile (e)) and the minor axis (profile (f)) of an ellipse of 0.9 eccentricity, and when the source is kept along the major axis of an ellipse of 0.4 eccentricity (profile (g)). As in Fig. 4, we show three object sizes: 1.5, 5, and 10 km halfwidth of geometrical shadow (indicated by dotted lines), for 1.7 km Fresnel scale. Results are the expected ones: a rapid change of the curvature at the immersion point strongly attenuates the diffraction fringes (profile (e)). The profile (f) is very near to the profile (c) of the opaque strip in Fig. 4, with very large fringes for the 1.5 km semiminor-axis case. For this large eccentricity, the Poisson spot virtually disappears, except for very small object areas. On the profile (g), the fringes are slightly attenuated compared to the circular case; the 1.5 km semimajor-axis object keeps the Poisson spot, but the 5 km object produces a central flash of only 0.5 intensity and the phenomenon almost disappears for the highest size.

observed with two telescopes from the ESO. One event appears simultaneously in the two recordings, and its width is greater than the stellar diameter and the Fresnel scale. We have studied it with our models and found that it is compatible with an occultation profile of a 1.4 km diameter circular object or with a ring of 0.7 km width and 0.6 km optical depth (Sicardy *et al.* 1986).

The 1980 occultation was observed with only one telescope. Six isolated events were detected that have the necessary width to be real (Sicardy *et al.* 1982). We have tested these events with our models: one of these dips is an artifact, and the other ones are compatible with rings or isolated moonlets (Roques *et al.*, in preparation).

At first sight, the occultation data processing requires knowledge of the stellar size. This parameter may be obtained from classical photometry methods. For outer planets, the apparent stellar diameter may range from 1 to 20 km, depending on the occulted star, so it smooths the diffraction profile of the rings (The Fresnel scale for the infrared wavelength used is about 1–2 km). However, the star radius can be considered, in the model, as an adjustable parameter, and thus the value given by the photometry can be confirmed or invalidated. As an example of such a method, we present a short analysis of our data of a Neptune arc profile, recorded at the ESO 0.5 m telescope.

The observation of an appulse of the star SAO 186001 by Neptune, on 22 July 1984, allowed the discovery of a Neptune ring arc (Hubbard *et al.* 1986). We recall that the event was observed at two different observatories in Chile, the CTIO and the ESO, separated by 100 km. A cross correlation of the two sets of observation data shows that the two events are virtually identical (Brahic *et al.*, in preparation; Roques 1986) and, from this similarity over a 100 km baseline, it is clear that a ring-like feature has been observed (which is denoted as an "arc" because of lack of continuity around the planet).

The best simulated profile obtained with the nominal star radius of 5 km shows a flat bottom not visible in the actual profile (Fig. 6(a)). If the star radius is an adjustable parameter, the best correlation (Fig. 7) is obtained with a star radius of 8.5 km, for which the synthetic profile correctly fits the data (Fig. 6(b)). The parameters of the ring are $w_n = 15$ km and $\tau_n = 0.68$. Arguments of Cuzzi (1985) for occultations by Uranus are also valid for this occultation, and, if

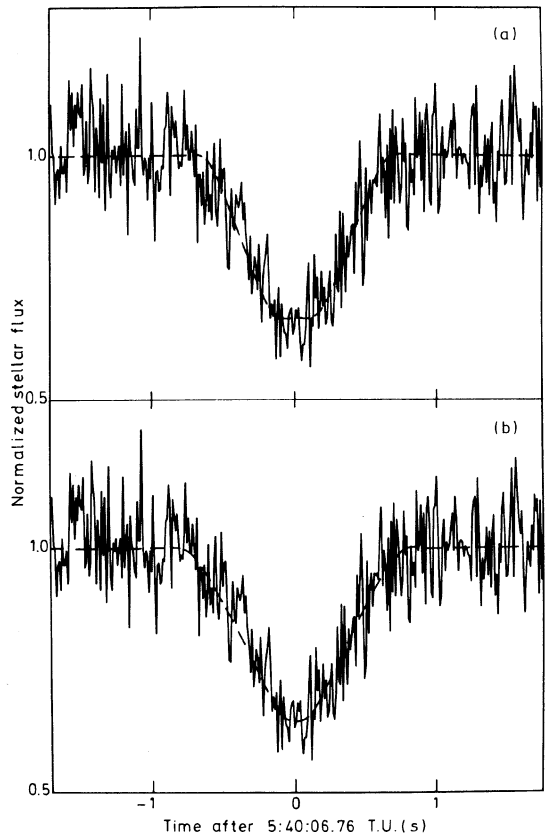


FIG. 6. Neptune arc profile, recorded at the ESO 0.5 m telescope on 22 July 1984, compared with the superposed theoretical profile (dotted line) for a 5 km star radius (profile (a)) and for an 8.5 km star radius (profile (b)).

*Voyager* should observe this arc, it will probably measure an optical depth reduced by half because of the abovementioned diffraction effect.

We have also fitted with the grey-strip model a Neptune arc(?) observed during the occultation of 20 August 1985

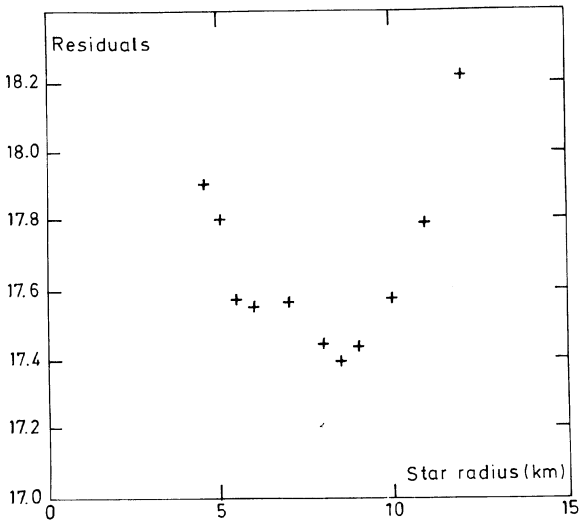


FIG. 7. Minima of the residuals obtained by fitting the Neptune arc profile with synthetic profiles for star radii between 4 and 12 km.

from the Canada-France-Hawaii Telescope. The curve giving residuals as a function of star radius shows two minima: A 4 km star radius corresponding to $w_n = 24.8$ km and $\tau_n = 0.08$, and a 6.5 km star radius corresponding to $w_n = 13.5$ km and $\tau_n = 0.15$. For star radii between 4 and 7 km, the equivalent width $w(1-f)$ of the best synthetic profile in the sky plane remains equal to 1.9 km (Sicardy *et al.*, in preparation).

## VI. CONCLUSIONS

We have considered here the Fresnel-Kirchhoff diffraction theory, from which we have derived some useful formulas: a formula for computing the grey-strip diffraction pattern and a method for computing the diffraction pattern of an opaque circular (or elliptical) object, based on the diffraction produced by a rectangular screen. Models based on these diffraction calculations allow one to distinguish, in occultation light curves, real events from spurious ones. We show that a ring composed of small particles which remove a fraction $f$ of the *energy* is observed from the Earth as a grey strip which removes a fraction $f$ of the *amplitude*. The fact explains why, as emphasized by Cuzzi (1985), the optical depth of the Uranian rings observed from the Earth is twice as much as from a close observation point. We show too that a ring occultation profile, analyzed with a diffraction model, can give a measure of the star diameter.

One of the goals of this paper was to present some efficient algorithms for modeling diffracting patterns observed during stellar occultations. Extensions of this work may be applied to more complicated situations than the square-well or elliptical models treated here:

(1) multibar models, using the additivity of amplitude, are easily derived from our square-well model. Many ring-occultation light curves are probably better fitted when using this kind of model. For instance, the 20 August 1985 occultation profile by an arc of Neptune observed at Canada-France-Hawaii Telescope clearly exhibits secondary structure extending over a few Fresnel scales.

(2) Figure 3 shows that diffraction patterns of small objects are easily derived from the Fresnel functions only. It would be of interest to generate diffraction patterns produced by a large number of small particles with a given size distribution law and compare the result with the *Voyager* PPS occultation experiment.

(3) Equation (11) implicitly assumes that the particles are randomly distributed. However, the diffraction pattern of a set of particles may be strongly affected by the pair correlation function of such particles. This may be the case for planetary rings where Keplerian motion and collisions do not distribute the particles randomly. This point deserves further investigation.

We thank André Brahic for helpful discussions, and William B. Hubbard for a careful reading of this paper.

## APPENDIX A: CALCULATION OF FRESNEL'S FUNCTIONS

$$C(x) = \int_0^x \cos\frac{1}{2}\pi t^2\,dt, \quad S(x) = \int_0^x \sin\frac{1}{2}\pi t^2\,dt.$$

Since we are dealing with odd functions, we may assume $x \geqslant 0$ and, to treat both integrals at once, we will describe the calculation of the complex Fresnel integral:

$$F(x) = \int_0^x e^{\frac{1}{2} i\pi t^2}\, dt = C(x) + iS(x)\,. \tag{A1}$$

From Eq. (A1), we have

$$F(x) = \int_0^{+\infty} e^{\frac{1}{2} i\pi t^2}\, dt + \frac{1}{2}\int_{+\infty}^{x^2} e^{\frac{1}{2} i\pi s} s^{-\frac{1}{2}}\, ds\,, \tag{A2}$$

and successive integrations by parts yield the asymptotic expansion of $F$:

$$F(x) = \frac{1}{2}(1+i) + e^{\frac{1}{2} i\pi x^2} \sum_{k=1}^{n} (-i)^k U_k(x) + R_n(x)\,, \tag{A3}$$

where

$$\begin{cases} U_1(x) = \dfrac{1}{\pi x} \\ U_{k+1}(x) = \dfrac{2k-1}{\pi x^2} U_k(x) \quad \text{for } k \geqslant 1\,, \end{cases} \tag{A4}$$

and

$$R_n(x) = (-i)^n U_n(x)(2n-1)x^{2n-1} \times \int_{+\infty}^{x} e^{\frac{1}{2} i\pi t^2} t^{-2n}\, dt\,. \tag{A5}$$

From Eq. (A5) we deduce that $|R_n(x)| < U_n(x)$ for any $n$, and since the real positive sequence $\{U_k(x)\}$ is decreasing if $(2k-1) < \pi x^2$, Eqs. (A3) and (A4) enable one to compute $F(x)$ with $\pm\epsilon$ accuracy if there exists an integer $k < (1/2)(\pi x^2 + 3)$ such that $U_k(x) < \epsilon$. So, for a given accuracy, there exists a lower limit of positive arguments $x$ for which the asymptotic expansion can be used (for example, if $\epsilon = 10^{-6}$, $x$ must be greater than 2.7). For smaller values, the simplest way is to use the regular series expansion

$$F(x) = x \sum_{k=0}^{\infty} i^k \frac{(\frac{1}{2}\pi x^2)^k}{k!(2k+1)} \tag{A6}$$

with $\pm$ accuracy reached when the absolute value of the last computed term is smaller than $\epsilon$. However, two difficulties are encountered when using this procedure: we cannot simply get any arbitrary accuracy because the switchover point from the regular to asymptotic series expansion depends on this accuracy, and, above all, the computation of terms of the series (A6) for $x$ such that $(1/2)\pi x^2 > 1$, requires many significant digits (11 digits if $\epsilon = 10^{-6}$). This arises because these terms first enormously increase in absolute values, compared to $|F(x)|$.

These difficulties are removed as follows: we compute the asymptotic expansion for any $x$ such that $(1/2)\pi x^2 \geqslant 1$ as long as the terms of the expansion decrease, and we estimate the remainder $R_n(x)$ of Eq. (A3) thanks to the regular series expansion (this expansion can be deduced from expansion 8.354,(2) in Gradshteyn and Ryzhik 1980):

$$R_n(x) = -\frac{1}{2}(1+i) + (-i)^n(2n-1)U_n(x) \times \sum_{k=0}^{\infty} i^k \frac{(\frac{1}{2}\pi x^2)^k}{k!(2k+1-2n)}\,. \tag{A7}$$

It is now possible to choose any accuracy: the remainder $R_n(x)$ is computed only if the asymptotic series expansion is not sufficient. To complete the algorithm in the case $(1/2)\pi x^2 < 1$, we carry in Eq. (A7) $U_0(x) = -x$, so $F(x) = (1/2)(1+i) + R_0(x)$, and we find again Eq. (A6).

## APPENDIX B: CALCULATION OF THE DIFFRACTION INTEGRAL FOR CIRCULAR SCREENS IN TERMS OF LOMMEL FUNCTIONS

In this Appendix, we shall evaluate the integral (9), which describes the diffracted amplitude produced by an opaque circular disk of radius $\rho$. The distance between the line of sight and the center of the disk is $r$, $D$ denotes the distance from the disk to the observer, and $\lambda$ is the observed wavelength. Expressing the lengths $r$ and $\rho$ in terms of Fresnel scale $\sqrt{\lambda D/2}$, the integral (9) becomes

$$a_\rho(r) = 1 + i\pi\, e^{\frac{1}{2} i\pi r^2} \int_0^{\rho} e^{\frac{1}{2} i\pi R^2} J_0(\pi r R) R\, dR\,. \tag{B1}$$

Using the well-known recursion relation between Bessel functions:

$$\frac{d}{dx}\left[x^{n+1} J_{n+1}(x)\right] = x^{n+1} J_n(x)\,,$$

and successively integrating by parts in Eq. (B1), we obtain (for further details about such a calculation, see Born and Wolf 1980, p. 435)

$$a_\rho(r) = 1 + e^{\frac{1}{2} i\pi(r^2+\rho^2)}[U_2(\rho,r) + iU_1(\rho,r)]\,, \tag{B2}$$

where $U_2$ and $U_1$ are the Lommel functions defined by

$$U_n(\rho,r) = \sum_{k=0}^{\infty} (-1)^k (\rho/r)^{n+2k} J_{n+2k}(\pi\rho r)\,. \tag{B3}$$

These series converge if $r \geqslant \rho$, so that Eq. (B2) provides the amplitude *outside* the geometrical shadow. In an analogous way, now using the recursion relation

$$\frac{d}{dx}\frac{[J_n(x)]}{x^n} = -\frac{J_{n+1}(x)}{x^n}$$

to integrate by parts in Eq. (B1), we obtain

$$a_\rho(r) = e^{\frac{1}{2} i\pi(r^2+\rho^2)}[U_0(r,\rho) - iU_1(r,\rho)]\,, \tag{B4}$$

which gives the amplitude *inside* the geometrical shadow. From the Eqs. (B2) and (B4), we obtain the following intensities:

if $r \geqslant \rho$:

$$I_\rho(r) = 1 + U_2^2(\rho,r) + U_1^2(\rho,r) + 2\{U_2(\rho,r)\cos\tfrac{1}{2}\pi(r^2+\rho^2) - U_1(\rho,r)\sin\tfrac{1}{2}\pi(r^2+\rho^2)\}\,, \tag{B5}$$

if $r \leqslant \rho$:

$$I_\rho(r) = U_0^2(r,\rho) + U_1^2(r,\rho)\,. \tag{B6}$$

The series (B3) converges rather slowly when $r \sim \rho$, i.e., near the edge of the geometrical shadow. However, the computation of $U_0$ and $U_1$ exactly on the shadow's boundary $r = \rho$ is simplified by identification with the expansions of cosine and sine in series of Bessel functions (Gradshteyn and Ryzhik 1980, formulas 8.514), i.e.,

$$U_0(\rho,\rho) = \tfrac{1}{2}[\cos(\pi\rho^2) + J_0(\pi\rho^2)]\,,$$
$$U_1(\rho,\rho) = \tfrac{1}{2}\sin(\pi\rho^2)\,,$$

so that

$$I_\rho(\rho) = \tfrac{1}{4}\left[J_0^2(\pi\rho^2) + 2\cos(\pi\rho^2)J_0(\pi\rho^2) + 1\right]. \quad \text{(B7)}$$

Another exact but obvious result of Eq. (B6) is $I_\rho(0) = 1$, i.e., the Poisson spot at the center of the geometrical shadow, discussed in the text.

Other analytical methods devised to evaluate the integral (9) are reviewed in Barakat (1961) and Boivin (1964).

## REFERENCES


Arlot, J.-E., Lecacheux, J., Richardson, Ch., and Thuillot, W. (1985). Icarus **61**, 224.

Barakat, R. (1961). In *Progress in Optics*, Vol. 1, edited by E. Wolf (Interscience, New York), p. 67.

Boivin, A. (1964). *Théorie et calcul des figures de diffraction de révolution* (Université Laval, Québec, and Gauthier-Villars, Paris), p. 413–428.

Born, M., and Wolf, E. (1980). *Principles of Optics*, 6th ed. (Pergamon, New York).

Cuzzi, J. N. (1985). Icarus **63**, 312.

Elliot, J. L. (1979). Annu. Rev. Astron. Astrophys. **17**, 445.

Elliot, J. L., Dunham, E., and Mink, D. (1977). Nature **267**, 328.

Elliot, J. L., French, R. G., Meech, K. J., and Elias, J. H. (1984). Astron. J. **89**, 1587.

Evans, D. S. (1970). Astron. J. **75**, 589.

Evans, D. S. (1984). Astron. J. **89**, 689.

French, R. G., Elliot, J. L., and Levine, S. E. (1986). Icarus **67**, 134.

Gradshteyn, I. S., and Ryzhik, I. M. (1980). *Table of Integrals, Series, and Products*, edited by A. Jeffrey (Academic, London).

Hubbard, W. B., Brahic, A., Sicardy, B., Elicer, L.-R., Roques, F., and Vilas, F. (1986). Nature **319**, 636.

Hubbard, W. B., and Zellner, B. H. (1980). Astron. J. **85**, 1663.

Lane, A. L., Hord, C. W., West, R. A., Esposito, L. W., Simmons, K. E., Nelson, R. M., Wallis, B. D., Buratti, B. J., Horn, L. J., Graps, A. L., and Pryor, W. R. (1986). Science **233**, 65.

Lecacheux, J. (1986). Private communication.

Lommel, E. (1884). Ab. Bayer. Akad. Wiss. **15**, 229.

Millis, R. L., Wasserman, L. H., Bowell, E., Franz, O. G., Klemola, A., and Dunham, D. W. (1984). Astron. J. **89**, 592.

Nather, R. E., and Evans, D. S. (1970). Astron. J. **75**, 575.

Nather, R. E., and McCants, M. M. (1970). Astron. J. **75**, 963.

Nicholson, P. D., Matthews, K., and Goldreich, P. (1982). Astron. J. **87**, 433.

Ridgway, S. T., Wells, D. C., Joyce, R. R., and Allen, R. G. (1979). Astron. J. **84**, 247.

Roques, F. (1986). Thèse de doctorat, Université Paris 7.

Sicardy, B., Combes, M., Brahic, A., Bouchet, P., Perrier, C., and Courtin, R. (1982). Icarus **52**, 454.

Sicardy, B., Roques, F., Brahic, A., Bouchet, P., Maillard, J. P., and Perrier, C. (1986). Nature **320**, 729.

White, N. M., and Slettebak, A. (1980). Astron. J. **85**, 44.